NUMERICAL SIMULATIONS OF TIME-FRACTIONAL PDES ARISING IN MATHEMATICS AND PHYSICS USING THE LOCAL MESHLESS DIFFERENTIAL QUADRATURE METHOD

by

Bander ALMUTAIRI[a], Imtiaz AHMAD[b], Bandar ALMOHSEN[a], Hijaz AHMAD[c,d*], and Dilber Uzun OZSAHIN[c,e]

[a] Department of Mathematics, College of Science, King Saud University, Riyadh, Saudi Arabia
[b] Department of Mathematics, University of Swabi, Khyber Pakhtunkhwa, Pakistan
[c] Operational Research Center in Healthcare, Near East University, Nicosia/Mersin, Turkey
[d] Section of Mathematics, International Telematic University Uninettuno, Roma, Italy
[e] Department of Medical Diagnostic Imaging, College of Health Sciences, Sharjah University, United Arab Emirates

Original scientific paper
https://doi.org/10.2298/TSCI23S1263A

The numerical solution of the 2-D time-fractional Sobolev equations is approximated using an efficient local differential quadrature method, in this paper. The time-fractional part of the model equations uses the Liouville-Caputo fractional derivative technique, however, the recommended meshless method is employed for the space derivatives. Test problems are used to undertake numerical experiments. In order to evaluate the effectiveness and accuracy of the suggested meshless method, we compared our outcomes with the exact solution and numerical methods presented in more recent literature. This comparison showed that the proposed method is more efficient computationally and yields excellent performance.

Key words: *meshless differential quadrature method, Caputo derivative, radial basis function, Sobolev equations, irregular domain*

Introduction

Recently, fractional partial differential equations (FPDE) got significant consideration. It emerged to become a cutting-edge tool for the more accurate description of many physical and technical processes. The FPDE contains the unknown multivariable function and its fractional partial derivatives. The FPDE are used to model problems with functions of several variables, to find solution of many physical models. Essential information about the fractional calculus can be found in [1]. We consider a class of 2-D Sobolev equations which are defined:

$$\frac{\partial^{\alpha} W(\overline{\mathbf{r}},t)}{\partial t^{\alpha}} - \frac{\partial \nabla^2 W(\overline{\mathbf{r}},t)}{\partial t} - \beta \nabla^2 W(\overline{\mathbf{r}},t) + \gamma \nabla \left(W(\overline{\mathbf{r}},t) \nabla W(\overline{\mathbf{r}},t) \right) + \delta W(\overline{\mathbf{r}},t) = F(\overline{\mathbf{r}},t)$$
$$\overline{\mathbf{r}} \in \Omega \subset \mathbb{R}^n, \ 0 < \alpha \leq 1, \ t > 0 \tag{1}$$

with the conditions:

$$W(\overline{\mathbf{r}},0) = W_0(\overline{\mathbf{r}}) \tag{2}$$

* Corresponding author, e-mail: hijaz555@gmail.com

$$W(\overline{\mathbf{r}},t) = g_1(\overline{\mathbf{r}},t),\ \ \overline{\mathbf{r}} \in \partial\Omega \tag{3}$$

where ∇^2 and ∇ represent the Laplacian gradient operators, respectively, and β, γ, δ are known constants. Moreover, $\partial^\alpha/\partial t^\alpha$ represent the Caputo derivative for $0 < \alpha \leq 1$, for $W(\overline{\mathbf{r}}, t)$which is defined [2]:

$$\frac{\partial^\alpha W(\overline{\mathbf{r}},t)}{\partial t^\alpha} = \begin{cases} \dfrac{1}{\Gamma(1-\alpha)} \displaystyle\int_0^t \frac{\partial W(\overline{\mathbf{r}},\vartheta)}{\partial \vartheta} (t-\vartheta)^{-\alpha}\, \mathrm{d}\vartheta, & 0 < \alpha < 1 \\ \dfrac{\partial W(\overline{\mathbf{r}},t)}{\partial t}, & \alpha = 1 \end{cases}$$

where $\Gamma(.)$ is the gamma function.

Meshless techniques have recently been shown to be effective tools for solving various PDE models in almost all disciplines of mathematics and physics. Meshless techniques based on the radial basis function (RBF) are the most common of these techniques. These techniques are particularly popular among researchers due to their meshless properties. These methods have the norm to circumvent the complication of dimensionality by utilizing conventional numerical techniques. Meshless techniques can be used to solve a variety of physical problems [3-6].

Meshless techniques have some limitations, the most significant of which is choosing the optimal shape-parameter value and dense ill-conditioned matrices. Researchers have developed the local meshless technique, which is effective and stable in solving a range of integer and fractional PDE models, to overcome these drawbacks [7, 8]. In comparison the global meshless version, these techniques are less sensitive to shape parameter selection and generate well-conditioned sparse matrices. Furthermore, the local meshless technique is less computationally expensive than its global version, making it more effective. These approaches have recently been tested in a variety of applications [9, 10].

The local differential quadrature method (LDQM) is included in this study to numerically simulate the time-fractional Model 1. In addition, numerical examinations take into account both regular and irregular domains.

Local differential quadrature scheme

In the proposed methodology, the derivatives of $W(\overline{\mathbf{r}}_h, t)$ are approximated at the centers $\overline{\mathbf{r}}_h$ by the neighborhood o $\overline{\mathbf{r}}_h$,

$$\{\overline{\mathbf{r}}_{h1}, \overline{\mathbf{r}}_{h2}, \overline{\mathbf{r}}_{h3}, ..., \overline{\mathbf{r}}_{hn_h}\} \subset \{\overline{\mathbf{r}}_1, \overline{\mathbf{r}}_2, \ldots, \overline{\mathbf{r}}_{N^n}\},\ n_h \ll N^n,\ \text{where}\ \ h = 1, 2..., N^n$$

In case of 1-D and 2-D case $\overline{\mathbf{r}} = x$ and $\overline{\mathbf{r}} = (x, y)$, respectively.

Procedure for 1-D case:

$$W^{(m)}(x_h) \approx \sum_{k=1}^{n_h} \lambda_k^{(m)} W(x_{hk}),\ \ h = 1, 2, \ldots, N \tag{4}$$

Substituting RBF $\psi(||x - x_p||)$ in eq. (4):

$$\psi^{(m)}\left(\left\|x_h - x_p\right\|\right) = \sum_{k=1}^{n_h} \lambda_{hk}^{(m)} \psi\left(\left\|x_{hk} - x_p\right\|\right),\ \ p = h_1, h_2, \ldots, hn_h \tag{5}$$

where for inverse multiquadric (IMQ) RBF, we have

$$\psi\left(\left\|x_{hk}-x_p\right\|\right)=1/\sqrt{1+\left(c\left\|x_{hk}-x_p\right\|\right)^2}$$

Matrix form of eq. (5):

$$\underbrace{\begin{bmatrix}\psi_{h1}^{(m)}(x_h)\\ \psi_{h2}^{(m)}(x_h)\\ \vdots\\ \psi_{hn_h}^{(m)}(x_h)\end{bmatrix}}_{\boldsymbol{\psi}_{n_h}^{(m)}}=\underbrace{\begin{bmatrix}\psi_{h1}(x_{h1}) & \psi_{h2}(x_{h1}) & \cdots & \psi_{hn_h}(x_{h1})\\ \psi_{h1}(x_{h2}) & \psi_{h2}(x_{h2}) & \cdots & \psi_{hn_h}(x_{h2})\\ \vdots & \vdots & \ddots & \vdots\\ \psi_{h1}(xh_{n_h}) & \psi_{h2}(x_{hn_h}) & \cdots & \psi_{hn_h}(xh_{n_h})\end{bmatrix}}_{\mathbf{A}_{n_h}}\underbrace{\begin{bmatrix}\lambda_{h1}^{(m)}\\ \lambda_{h2}^{(m)}\\ \vdots\\ \lambda_{hn_h}^{(m)}\end{bmatrix}}_{\boldsymbol{\lambda}_{n_h}^{(m)}} \tag{6}$$

where

$$\psi_p(x_k)=\psi(\|x_k-x_p\|),\ p=h_1,h_2,\ldots,hn_h,$$

for each $k = h_1, h_2,...h_{n_h}$. Equation (6) can be written:

$$\psi_{n_h}^{(m)}=\mathbf{A}_{n_h}\boldsymbol{\lambda}_{n_h}^{(m)} \tag{7}$$

From eq. (7), we obtain:

$$\boldsymbol{\lambda}_{n_h}^{(m)}=\mathbf{A}_{n_h}^{-1}\psi_{n_h}^{(m)} \tag{8}$$

eqs. (4) and (8) imply

$$W^{(m)}(x_h)=\left(\boldsymbol{\lambda}_{n_h}^{(m)}\right)^T\mathbf{W}_{n_h}$$

where

$$\mathbf{W}_{n_h}=\left[W(x_{h1}),W(x_{h2}),\ldots,W(x_{hn_h})\right]^T$$

The derivatives of $W(x, y, t)$ w.r.t. x and y can be found:

$$W_x^{(m)}(x_h,y_h)\approx\sum_{k=1}^{n_h}\gamma_k^{(m)}W(x_{hk},y_{hk}),\quad h=1,2,\ldots,N^2$$

$$W_y^{(m)}(x_h,y_h)\approx\sum_{k=1}^{n_h}\eta_k^{(m)}W(x_{hk},y_{hk}),\quad h=1,2,\ldots,N^2$$

For $\gamma_k^{(m)}$ and $\eta_k^{(m)}$ ($k = 1, 2,..., n_h$), we continue:

$$\boldsymbol{\gamma}_{n_h}^{(m)}=\mathbf{A}_{n_h}^{-1}\boldsymbol{\Phi}_{n_h}^{(m)}$$

$$\eta_{n_h}^{(m)}=\mathbf{A}_{n_h}^{-1}\boldsymbol{\Phi}_{n_h}^{(m)}$$

Similar procedure can be adopted for 3-D case.

Figure 1 depicts the construction of local stencils around each center $\bar{\mathbf{r}}_h$ in 2-D domains, whereas fig. 2 depicts the sparsity pattern of the LDQM for five and seven stencils.

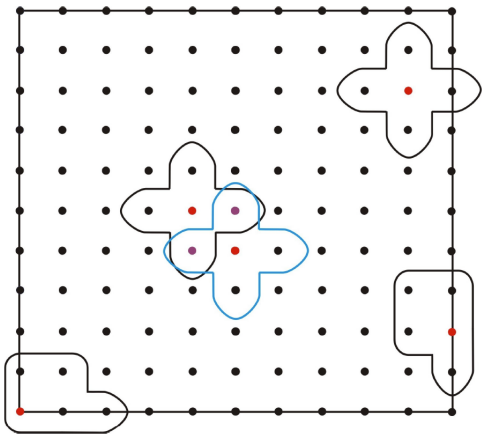

Figure 1. Schematics view in 2-D for local stencil five

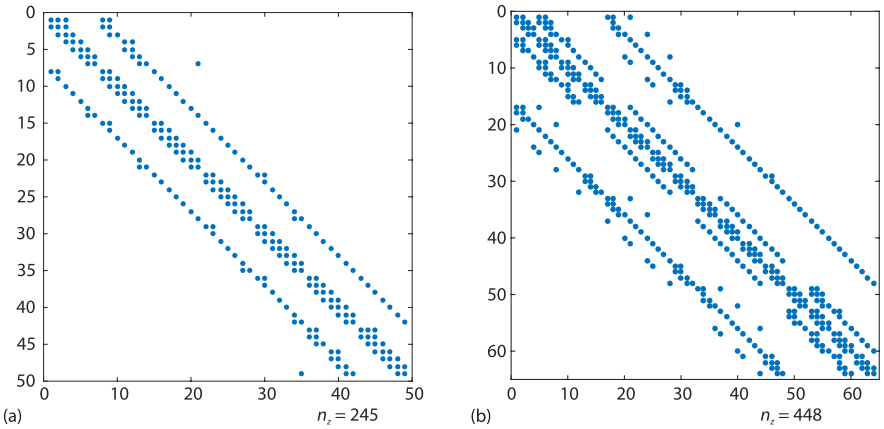

Figure 2. Sparsity pattern of the LDQM in (a) 2-D and (b) 3-D for local stencil five and seven, respectively

Time discretization

The Caputo derivative [2] is utilized for time-fractional derivative:

$$\frac{\partial^{\alpha} W(\bar{\mathbf{r}},t)}{\partial t^{\alpha}} \quad \text{for} \quad \alpha \in (0,1)$$

as

$$\frac{\partial^{\alpha} W(\bar{\mathbf{r}},t)}{\partial t^{\alpha}} = \begin{cases} \dfrac{1}{\Gamma(1-\alpha)} \displaystyle\int_0^t \frac{\partial W(\bar{\mathbf{r}},\vartheta)}{\partial \vartheta} (t-\vartheta)^{-\alpha} \, \mathrm{d}\vartheta, & 0 < \alpha < 1 \\ \dfrac{\partial W(\bar{\mathbf{r}},t)}{\partial t}, & \alpha = 1 \end{cases}$$

We can obtain the derivative term as follows, where $t_q = q\tau$, $q = 0, 1, 2..., Q$, and time step size $\Delta\tau$ in $[0, t]$:

$$\frac{\partial^\alpha W(\overline{\mathbf{r}},t_{q+1})}{\partial t^\alpha}=\frac{1}{\Gamma(1-\alpha)}\int_0^{t_{q+1}}\frac{\partial W(\overline{\mathbf{r}},\vartheta)}{\partial\vartheta}\left(t_{q+1}-\vartheta\right)^{-\alpha}\,\mathrm{d}\vartheta=$$

$$=\frac{1}{\Gamma(1-\alpha)}\sum_{s=0}^{q}\int_{s\tau}^{(s+1)\tau}\frac{\partial W(\overline{\mathbf{r}},\vartheta)}{\partial\vartheta}\left(t_{s+1}-\vartheta\right)^{-\alpha}\,\mathrm{d}\vartheta\approx$$

$$\approx\frac{1}{\Gamma(1-\alpha)}\sum_{s=0}^{q}\int_{s\tau}^{(s+1)\tau}\frac{\partial W(\overline{\mathbf{r}},\vartheta_s)}{\partial\vartheta}\left(t_{s+1}-\vartheta\right)^{-\alpha}\,\mathrm{d}\vartheta$$

The term

$$\frac{\partial W(\overline{\mathbf{r}},\vartheta_s)}{\partial\vartheta}\ \text{can be approximate as}\ \frac{\partial W(\overline{\mathbf{r}},\vartheta_s)}{\partial\vartheta}=\frac{W(\overline{\mathbf{r}},\vartheta_{s+1})-W(\overline{\mathbf{r}},\vartheta_s)}{\vartheta}+\mathcal{O}(\tau)$$

Then

$$\frac{\partial^\alpha W(\overline{\mathbf{r}},t_{q+1})}{\partial t^\alpha}\approx\frac{1}{\Gamma(1-\alpha)}\sum_{s=0}^{q}\frac{W(\overline{\mathbf{r}},t_{s+1})-W(\overline{\mathbf{r}},t_s)}{\tau}\int_{s\tau}^{(s+1)\tau}\left(t_{s+1}-\vartheta\right)^{-\alpha}\,\mathrm{d}\vartheta=$$

$$=\frac{1}{\Gamma(1-\alpha)}\sum_{s=0}^{q}\frac{W(\overline{\mathbf{r}},t_{q+1-s})-W(\overline{\mathbf{r}},t_{q-s})}{\tau}\int_{s\tau}^{(s+1)\tau}\left(t_{s+1}-\vartheta\right)^{-\alpha}\,\mathrm{d}\vartheta=$$

$$=\begin{cases}\dfrac{\tau^{-\alpha}}{\Gamma(2-\alpha)}(W^{q+1}-W^q)+\dfrac{\tau^{-\alpha}}{\Gamma(2-\alpha)}\displaystyle\sum_{s=1}^{q}(W^{q+1-s}-W^{q-s})[(s+1)^{1-\alpha}-s^{1-\alpha}], & q\geq 1\\ \dfrac{\tau^{-\alpha}}{\Gamma(2-\alpha)}\left(W^1-W^0\right) & q=0\end{cases}$$

Letting:

$$a_0=\frac{\tau^{-\alpha}}{\Gamma(2-\alpha)}\ \text{ and }\ b_s=\left(s+1\right)^{1-\alpha},\ s=0,1,...,q$$

we have:

$$\frac{\partial^\alpha W(\overline{\mathbf{r}},t_{q+1})}{\partial t^\alpha}\approx\begin{cases}a_0\left(W^{q+1}-W^q\right)+a_0\displaystyle\sum_{s=1}^{q}b_s\left(W^{q+1-s}-W^{q-s}\right), & q\geq 1\\ a_0\left(W^1-W^0\right), & q=0\end{cases}\tag{9}$$

Numerical discussion

The proposed LDQM is evaluated for its ability to accurately and efficiently approximate the solution of model equation (1). Two test problems are considered with uniform and scatted nodes with non-rectangular and rectangular domains. Throughout the paper, we have used IMQ RBF with shape parameter value $c = 15 \cdot 10^5$. The local stencil five in the spatial domain [0, 4] are utilized unless mentioned explicitly. For accuracy measurement, we used the error norms:

$$\max(\varepsilon) = \max\left(\left|\widehat{\mathbb{W}} - W\right|\right)$$
$$RMS = \sqrt{\frac{\sum_{i=1}^{N}\left(\widehat{\mathbb{W}}_i - W_i\right)^2}{N}} \tag{10}$$

where W is the approximate solution and $\widehat{\mathbb{W}}$ – the exact solution.

Test Problem 1. The exact solution of Model 1 with $\beta = 1$, $\gamma = \delta = 0$:

$$W(\bar{\mathbf{r}},t) = \mathrm{e}^{-t}\sin(\pi x)\sin(\pi y),\ \ \bar{\mathbf{r}} = (x,y) \in \Omega \tag{11}$$

where

$$F(\bar{\mathbf{r}},t) = -t^{(1-\alpha)}\mathfrak{M}_{1,2-\alpha} - t\sin(\pi x)\sin(\pi y) \tag{12}$$

where $\mathfrak{M}_{1,2-\alpha}$ is Mittag-Leffler function of two parameters as defined in [11].

The proposed LDQM is utilized to approximate the numerical results for *Test Problem 1* and listed in tab. 1-3. In tab. 1, different values of α, nodal points N, time step size $\tau = 0.0005$ and final time $t = 1$ are used to computed the results. In viewed the tabulated results, very good agreement with the exact solution can be seen. Furthermore, the LDQM delivers better results than the method mentioned in [11]. Also, we note that the LDQM produced ideal well-conditioned coefficient matrices. In tab. 2, results are computed in form of RMS by taking $N = 10^2$ and different values of fractional order α, τ, and t. We observed that the accuracy increases with decrease time step size τ to some extend. In tab. 3, comparison is made between the present LDQM with the methods given in [12-14] for $\alpha = 1$, $t = 1$, $\tau = 0.01$ and spatial domain [0, 1] in term of max(ε). One can found that the present method produced better results than the methods given in [12-14].

Table 1. *Test Problem 1*, results of the LDQM

		$\alpha = 0.2$		$\alpha = 0.5$		$\alpha = 0.8$		
N	Method	max(ε)	*RMS*	max(ε)	*RMS*	max(ε)	*RMS*	Condition No.
10^2	LDQM	$7.432 \cdot 10^{-9}$	$3.448 \cdot 10^{-9}$	$7.432 \cdot 10^{-9}$	$3.448 \cdot 10^{-9}$	$7.432 \cdot 10^{-9}$	$3.448 \cdot 10^{-9}$	1.0000
	[11]	$7.664 \cdot 10^{-7}$	$3.484 \cdot 10^{-7}$	$7.664 \cdot 10^{-7}$	$3.484 \cdot 10^{-7}$	$7.664 \cdot 10^{-7}$	$3.484 \cdot 10^{-7}$	
20^2	LDQM	$7.611 \cdot 10^{-9}$	$3.640 \cdot 10^{-9}$	$7.611 \cdot 10^{-9}$	$3.640 \cdot 10^{-9}$	$7.611 \cdot 10^{-9}$	$3.640 \cdot 10^{-9}$	1.0000
	[11]	$7.664 \cdot 10^{-7}$	$3.650 \cdot 10^{-7}$	$7.664 \cdot 10^{-7}$	$3.650 \cdot 10^{-7}$	$7.664 \cdot 10^{-7}$	$3.650 \cdot 10^{-7}$	
25^2	LDQM	$7.633 \cdot 10^{-9}$	$3.684 \cdot 10^{-9}$	$7.633 \cdot 10^{-9}$	$3.684 \cdot 10^{-9}$	$7.633 \cdot 10^{-9}$	$3.684 \cdot 10^{-9}$	1.0000
	[11]	$7.634 \cdot 10^{-7}$	$3.685 \cdot 10^{-9}$	$7.634 \cdot 10^{-7}$	$3.685 \cdot 10^{-7}$	$7.634 \cdot 10^{-7}$	$3.685 \cdot 10^{-7}$	

Table 2. *Test Problem 1*, results of the LDQM using $N = 10^2$

RMS						
	$t = 5$			$t = 10$		
τ	$\alpha = 0.1$	$\alpha = 0.5$	$\alpha = 0.9$	$\alpha = 0.1$	$\alpha = 0.5$	$\alpha = 0.9$
0.5	$3.11 \cdot 10^{-4}$	$3.1110 \cdot 10^{-4}$	$3.1110 \cdot 10^{-4}$	$3.9772 \cdot 10^{-6}$	$3.9772 \cdot 10^{-6}$	$3.9773 \cdot 10^{-6}$
0.05	$3.1579 \cdot 10^{-6}$	$3.1580 \cdot 10^{-6}$	$3.1580 \cdot 10^{-6}$	$4.2523 \cdot 10^{-8}$	$4.2529 \cdot 10^{-8}$	$4.2531 \cdot 10^{-8}$
0.005	$3.1582 \cdot 10^{-8}$	$3.1582 \cdot 10^{-8}$	$3.1583 \cdot 10^{-8}$	$4.1499 \cdot 10^{-10}$	$4.2034 \cdot 10^{-10}$	$4.2281 \cdot 10^{-10}$
0.0005	$3.1339 \cdot 10^{-10}$	$3.1421 \cdot 10^{-10}$	$3.1466 \cdot 10^{-10}$	$6.3729 \cdot 10^{-12}$	$1.0264 \cdot 10^{-12}$	$1.4410 \cdot 10^{-12}$

Table 3. *Test Problem 1*, comparison of the simulation results of the LDQM and [12-14]

	Max(ε)			
N	LDQM	[12]	[13]	[14]
4^2	$3.065 \cdot 10^{-6}$	$4.2735 \cdot 10^{-4}$	$7.4767 \cdot 10^{-3}$	$3.067 \cdot 10^{-6}$
8^2	$3.065 \cdot 10^{-6}$	$1.4656 \cdot 10^{-4}$	$2.1515 \cdot 10^{-3}$	$3.067 \cdot 10^{-6}$
16^2	$3.065 \cdot 10^{-6}$	$1.2647 \cdot 10^{-5}$	$4.9543 \cdot 10^{-4}$	$3.067 \cdot 10^{-6}$

To test the proposed method on non-rectangular domains with uniform and non-uniform data points are shown in figs. 3-5 for *Test Problem 1* with $\alpha = 0.5$, $\tau = 0.0005$, and $t = 1$. These figures show acceptable accuracy regardless of the computational domains.

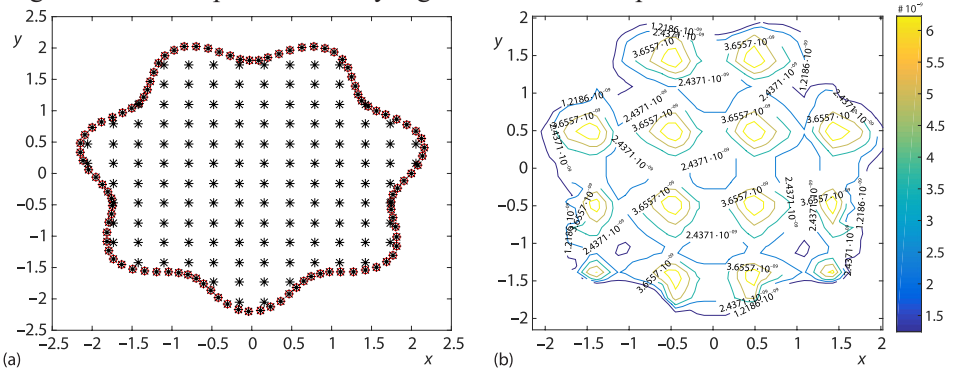

Figure 3. *Test Problem 1*; (a) domain and (b) absolute error with $N = 229$

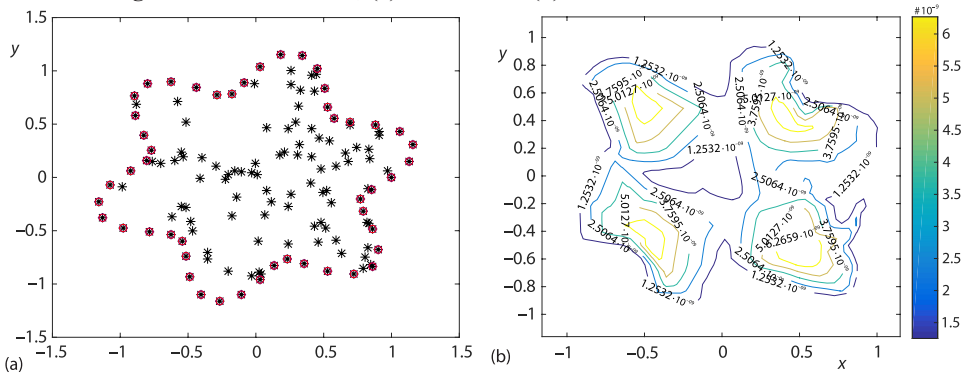

Figure 4. *Test Problem 1*; (a) domain and (b) absolute error with $N = 135$

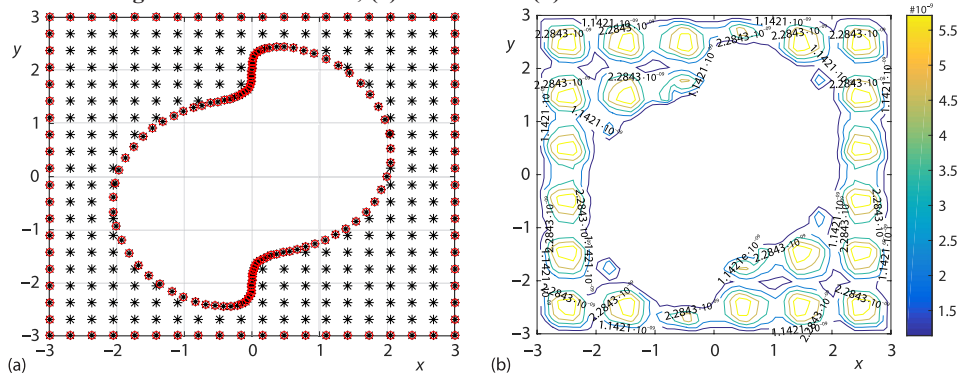

Figure 5. *Test Problem 1*; (a) domain and (b) absolute error with $N = 229$

The numerical stability of the proposed LDQM as revealed in [9] is shown in figs. 6-8. In spite of the fact that the stability of the meshless method using shape parameter-dependent RBF is impacted heavily by the numbers of nodes N and shape parameter c. The values of c and N have a huge impact on the accuracy and conditional number of the global meshless approach, according to the literature, and the system becomes ill-conditioned [11, 14]. The current LDQM, on the other hand, is tested for a large range of c (up to $2 \cdot 10^6$) and N (up to 602) and shows steady behaviour as shown in figs. 6-8. Additionally, the condition number of the coefficient matrices are ideal and is around to one as shown in figs. 7(b) and 8(b).

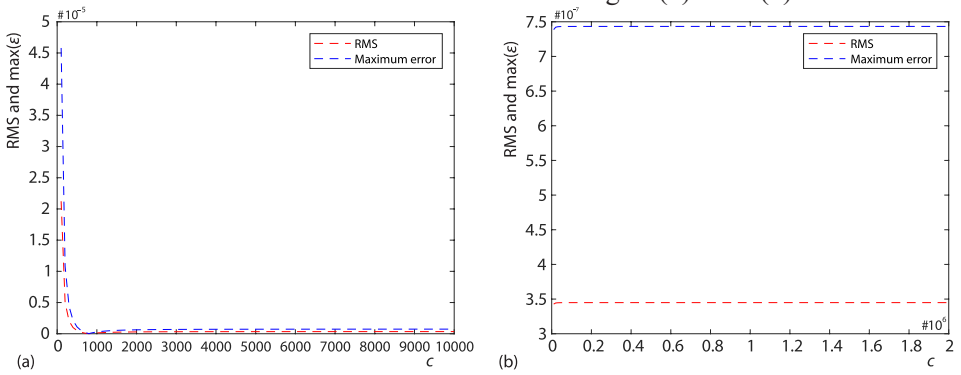

Figure 6. *Test Problem 1*, shape parameter c *vs.* RMS and max(ε) using $\alpha = 0.5$, $N = 10^2$, $t = 1$

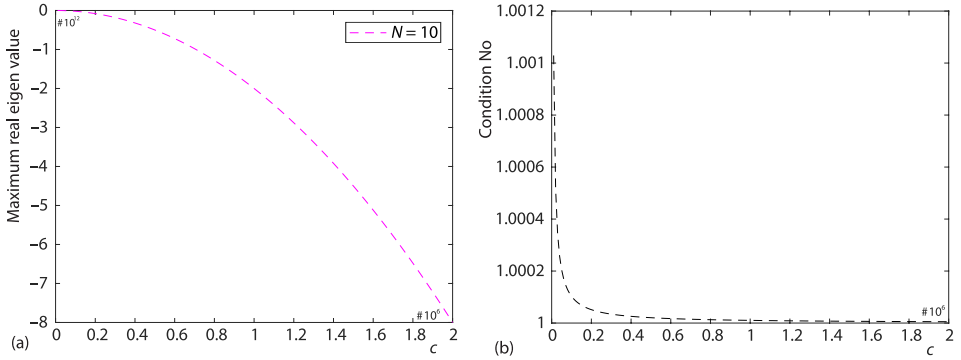

Figure 7. *Test Problem 1*, (a) shape parameter c *vs.* maximum eigen value and (b) shape parameter c *vs.* condition number using $\alpha = 0.5$, $N = 10^2$, $\tau = 0.005$, $t = 1$

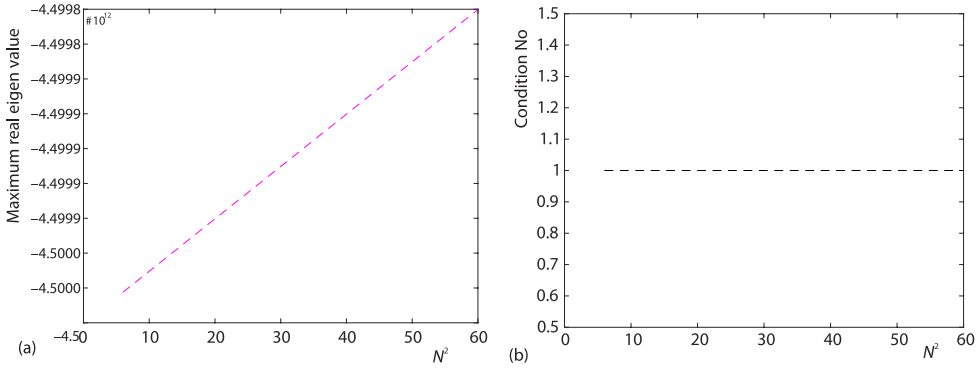

Figure 8. *Test Problem 1*, (a) number of nodes N *vs.* maximum eigen value and (b) N *vs.* condition number using $\alpha = 0.5$, $\tau = 0.005$, $t = 1$

Test Problem 2. The exact solution for the Model 1 with $\beta = 1$, $\gamma = 1$, $\delta = \pi^2$ is given:

$$W(\bar{\mathbf{r}},t) = \mathrm{e}^t \sin(\pi x)\sin(\pi y), \quad \bar{\mathbf{r}} = (x, y) \in \Omega \tag{13}$$

Figure 9 shows the good agreement between the exact and numerical solution of the LDQM for *Test Problem 2* using $\alpha = 0.5$, $N = 20^2$, $\tau = 0.005$ and time $t = 0.2$.

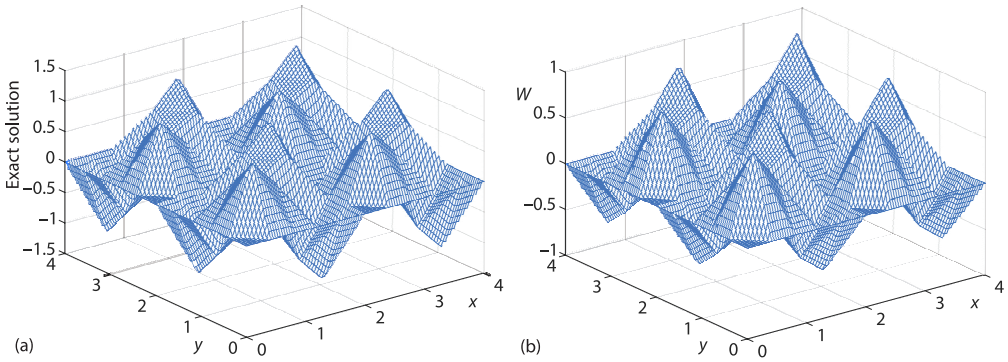

Figure 9. *Test Problem 2*, (a) exact solution and (b) numerical solution

Conclusion

In order to explore 2-D time-fractional Sobolev equations, we have employed a realistic numerical technique termed the local differential quadrature algorithm based on radial basis functions. The problem is discretized in the time direction using the Crank-Nicolson time-integration method first, and then the local differential quadrature method is applied. In comparison methods described in recent literature, the current method constructed a sparse linear system of equations with an ideal lower condition number and accurately approximated the solution.

Acknowledgment

Authors extend their appreciate to the Deanship of Scientific Research at King Saud University for funding this work through research group no RG-1441-327.

References

[1] Diethelm, K., *The Analysis of Fractional Differential Equations: An Application-Oriented Exposition Using Differential Operators of Caputo Type*, Springer Science and Business Media, Berlin, Germany, 2010
[2] Caputo, M., Linear Models of Dissipation whose Q is Almost Frequency Independent – II, *Geophysical Journal International*, *13* (1967) 5, pp. 529-539
[3] Wang, F., *et al*., Gaussian Radial Basis Functions Method for Linear and Non-Linear Convection-Diffusion Models in Physical Phenomena, *Open Physics*, *19* (2021) 1, pp. 69-76
[4] Wang, F., *et al.*, Formation of Intermetallic Phases in Ion Implantation, *Journal of Mathematics*, *2020* (2020), ID8875976
[5] Nawaz, R., *et al*., An Extension of Optimal Auxiliary Function Method to Fractional Order High Dimensional Equations, *Alexandria Engineering Journal*, *60* (2021) 5, pp. 4809-4818
[6] Ahmad, I., *et al*., Application of Local Meshless Method for the Solution of Two Term Time Fractional-Order Multi-Dimensional PDE Arising in Heat and Mass Transfer, *Thermal Science*, *24* (2020), Suppl. 1, pp. S95-S105
[7] Ahmad, I., *et al*., Numerical Simulation of PDE by Local Meshless Differential Quadrature Collocation Method, *Symmetry*, *11* (2019) 3, 394
[8] Ahmad, I., *et al.*, An Efficient Local Formulation for Time-Dependent PDE, *Mathematics*, *7* (2019), 216

[9] Ahmad, I., *et al*., Local RBF Method for Multi-Dimensional Partial Differential Equations, Computers and *Mathematics with Applications*, *74* (2017), 2, pp. 292-324
[10] Shu, C., *Differential Quadrature and Its application in Engineering*, Springer, London, UK, 2000
[11] Haq, S., Hussain, M., Application of Meshfree Spectral Method for the Solution of Multi-Dimensional Time-Fractional Sobolev Equations, *Engineering Analysis with Boundary Elements*, *106* (2019), Sept., pp. 201-216
[12] Oruc, O., A Computational Method Based on Hermite Wavelets for 2-D Sobolev and Regularized Long Wave Equations in Fluids, *Numerical Methods for Partial Differential Equations*, *34* (2018) 5, pp. 1693-1715
[13] Haq, S., *et al*., Numerical Solutions of 2-D Sobolev and Generalized Benjamin-Bona-Mahony-Burgers' Equations Via Haar Wavelets, *Computers and Mathematics with Applications*, *77* (2019), 2, pp. 565-575
[14] Hussain, M., *et al*., Meshless RBF method for numerical solutions of 2-D high order fractional Sobolev equations, *Computers and Mathematics with Applications*, *79* (2020) 3, pp. 802-816

Paper submitted: April 21, 2022
Paper revised: May 24, 2022
Paper accepted: June 4, 2022